# Quantifying the nitrogen isotope effects during photochemical equilibrium between NO and $NO_2$: implications for $\delta^{15}N$ in tropospheric reactive nitrogen

Jianghanyang Li[1], Xuan Zhang[2], John Orlando[2], Geoffrey Tyndall[2] and Greg Michalski[1,3]

[1.] Department of Earth, Atmospheric and Planetary Sciences, Purdue University, West Lafayette, IN, 47907
[2.] Atmospheric Chemistry Observations and Modeling Lab, National Center for Atmospheric Research, Boulder, CO, 80301
[3.] Department of Chemistry, Purdue University, West Lafayette, IN, 47907

*Correspondence to*: Jianghanyang Li (li2502@purdue.edu)

**Abstract.** Nitrogen isotope fractionations between nitrogen oxides (NO and $NO_2$) play a significant role in determining the nitrogen isotopic compositions ($\delta^{15}N$) of atmospheric reactive nitrogen. Both the equilibrium isotopic exchange between NO and $NO_2$ molecules and the isotope effects occurring during the $NO_x$ photochemical cycle are important, but both are not well constrained. The nighttime and daytime isotopic fractionations between NO and $NO_2$ in an atmospheric simulation chamber at atmospherically relevant $NO_x$ levels were measured. Then, the impact of $NO_x$ level and $NO_2$ photolysis rate to the combined isotopic fractionation (equilibrium isotopic exchange and photochemical cycle) between NO and $NO_2$ were calculated. It was found that the isotope effects occurring during the $NO_x$ photochemical cycle can be described using a single fractionation factor, designated the Leighton Cycle Isotope Effect (LCIE). The results showed that at room temperature, the fractionation factor of nitrogen isotopic exchange is 1.0275±0.0012, and the fractionation factor of LCIE (when $O_3$ solely controls the oxidation from NO to $NO_2$) is 0.990±0.005. The measured LCIE factor showed good agreement with previous field measurements, suggesting that it could be applied in ambient environment, although future work is needed to assess the isotopic fractionation factors of NO + $RO_2/HO_2 \rightarrow NO_2$. The results were used to model the NO-$NO_2$ isotopic fractionations under several $NO_x$ conditions. The model suggested that isotopic exchange was the dominate factor when $NO_x$ >20 nmol $mol^{-1}$, while LCIE was more important at low $NO_x$ concentrations (<1 nmol $mol^{-1}$) and high rates of $NO_2$ photolysis. These findings provided a useful tool to quantify the isotopic fractionations between tropospheric NO and $NO_2$, which can be applied in future field observations and atmospheric chemistry models.

## 1. Introduction

The nitrogen isotopic composition ($\delta^{15}N$) of reactive nitrogen compounds in the atmosphere is an important tool in understanding the sources and chemistry of atmospheric $NO_x$ ($NO+NO_2$). It has been suggested that the $\delta^{15}N$ value of atmospheric nitrate ($HNO_3$, nitrate aerosols and nitrate ions in the precipitation and snow) imprints the $\delta^{15}N$ value of $NO_x$ sources (Elliott et al., 2009; Kendall et al., 2007) thus many studies have used the $\delta^{15}N$ values of atmospheric nitrate to investigate $NO_x$ sources (Chang et al., 2018; Felix et al., 2012; Felix & Elliott, 2014; Gobel et al., 2013; Hastings et al., 2004, 2009; Morin et al., 2009; Park et al., 2018; Walters et al., 2015, 2018). However, there remain questions about how isotopic fractionations that may occur during photochemical cycling of $NO_x$ could alter the $\delta^{15}N$ values as it partitions into $NO_y$ ($NO_y$ = atmospheric nitrate, $NO_3$, $N_2O_5$, HONO, etc., Chang et al., 2018; Freyer, 1991; Hastings et al., 2004; Jarvis et al., 2008; Michalski et al., 2005; Morin et al., 2009; Zong et al., 2017). Similarily, other complex reactive nitrogen chemistry, such as nitrate photolysis and re-deposition in ice and snow (Frey et al., 2009), may impact the $\delta^{15}N$ of $NO_y$ and atmospheric nitrate. The fractionation between NO and $NO_2$ via isotope exchange has been suggested to be the dominant factor in determining the $\delta^{15}N$ of $NO_2$ and ultimately atmospheric nitrate (Freyer, 1991; Freyer et al., 1993; Savarino et al., 2013; Walters et al., 2016). However, isotopic fractionations occur in most, if not all, $NO_x$ and $NO_y$ reactions, while most of these are still unknown or, if calculated (Walters and Michalski, 2015), unverified by experiments. Since the atmospheric chemistry of $NO_y$ varies significantly in different environments (e.g., polluted vs. pristine, night vs. day), the isotopic fractionations associated with $NO_y$ chemistry are also likely to vary in different environments. These unknowns could potentially bias conclusions about $NO_x$ source apportionment reached when using nitrogen isotopes. Therefore, understanding the isotopic

fractionations between NO and $NO_2$ during photochemical cycling could improve our understanding of the relative role of sources versus chemistry for controlling the $\delta^{15}N$ variations of atmospheric $NO_2$ and nitrate.

In general, there are three types of isotopic fractionation effects associated with $NO_x$ chemistry (Fig. 1A). The first type is the equilibrium isotopic effect (EIE), i.e., isotope exchange between two compounds without forming new molecules (Urey, 1947, Bigeleisen and Mayer, 1947), which for nitrogen isotopes in the $NO_x$ system is the $^{15}NO + {}^{14}NO_2 \leftrightarrow {}^{14}NO + {}^{15}NO_2$ exchange reaction (Begun and Melton, 1956, Walters et al., 2016). The second type is the kinetic isotopic effect (KIE) associated with difference in isotopologue rate coefficients during unidirectional reactions (Bigeleisen & Wolfsberg, 1957). In the $NO_x$ system this KIE would manifest in the oxidation of NO into $NO_2$ by $O_3/HO_2/RO_2$. The third type is the photochemical isotope fractionation effect (PHIFE, Miller & Yung, 2000), which for $NO_x$ is the isotopic fractionation associated with $NO_2$ photolysis. All three fractionations could impact the $\delta^{15}N$ value of $NO_2$, and consequently atmospheric nitrate, but the relative importance of each may vary.

The limited number of studies on the EIE in the $NO_x$ cycle have significant uncertainties. Discrepancies in the EIE for $^{15}NO + {}^{14}NO_2 \leftrightarrow {}^{14}NO + {}^{15}NO_2$ have been noted in several studies. Theoretical calculations predicted isotope fractionation factors ($\alpha$) ranging from 1.035 to 1.042 at room temperature (Begun & Fletcher, 1960; Monse et al., 1969; Walters & Michalski, 2015) due to the different approximations used to calculate harmonic frequencies in each study. Likewise, two separate experiments measured different room temperature fractionation factors of 1.028±0.002 (Begun & Melton, 1956) and 1.0356±0.0015 (Walters et al., 2016). A concern in both experiments is that they were conducted in small chambers with high $NO_x$ concentrations (hundreds of μmol $mol^{-1}$), significantly higher than typical ambient atmospheric $NO_x$ levels

(usually less than 0.1 μmol $mol^{-1}$). Whether the isotopic fractionation factors determined by these experiments are applicable in the ambient environment is uncertain because of possible wall effects and formation of higher oxides, notably $N_2O_4$ and $N_2O_3$ at these high $NO_x$ concentrations.

Even less research has examined the KIE and PHIFE occurring during $NO_x$ cycling. The KIE of NO + $O_3$ has been theoretically calculated (Walters and Michalski, 2016) but has not been experimentally verified. The $NO_2$ PHIFE has not been experimentally determined or theoretically calculated. As a result, field observation studies often overlook the effects of PHIFE and KIE. Freyer et al. (1993) measured $NO_x$ concentrations and the $\delta^{15}N$ values of $NO_2$ over a 1-year period at Julich, Germany and inferred a combined $NO_x$ isotope fractionation factor (EIE+KIE+PHIFE) of 1.018±0.001. Freyer et al. (1993) suggested that the $NO_x$ photochemical cycle (KIE and PHIFE) tends to diminish the equilibrium isotopic fractionation (EIE) between NO and $NO_2$. Even if this approach were valid, applying this single fractionation factor elsewhere, where $NO_x$, $O_3$ concentrations and actinic fluxes are different, would be tenuous given that these factors may influence the relative importance of EIE, KIE and PHIFE (Hastings et al., 2004; Walters et al., 2016). Therefore, to quantify the overall isotopic fractionations between NO and $NO_2$ at various tropospheric conditions, it is crucial to know 1) isotopic fractionation factors of EIE, KIE and PHIFE individually and 2) the relative importance of each factor under various conditions.

In this work, we aim to quantify the nitrogen isotope fractionation factors between NO and $NO_2$ at photochemical equilibrium. First, we measure the N isotope fractionations between NO and $NO_2$ in an atmospheric simulation chamber at atmospherically relevant $NO_x$ levels. Then, we provide mathematical solutions to assess the impact of $NO_x$ level and $NO_2$ photolysis rate ($j(NO_2)$) to the relative importance of EIE, KIE and PHIFE. Subsequently we use the solutions and chamber measurements to calculate the isotopic fractionation factors of EIE, KIE and PHIFE. Lastly, using

the calculated fractionation factors and the equations, we model the NO-$NO_2$ isotopic fractionations at several sites to illustrate the behavior of $\delta^{15}N$ values of $NO_x$ in the ambient environment.

## 2. Methods

The experiments were conducted using a 10 $m^3$ Atmospheric Simulation Chamber at the National Center for Atmospheric Research (see descriptions in Appendix A and Zhang et al. (2018)). A set of mass flow controllers was used to inject NO and $O_3$ into the chamber. NO was injected at 1 L $min^{-1}$ from an in-house NO/$N_2$ cylinder (133.16 μmol $mol^{-1}$ NO in ultra-pure $N_2$), and $O_3$ was generated by flowing 5 L $min^{-1}$ zero-air through a flow tube equipped with a UV Pen-Ray lamp (UVP LLC., CA) into the chamber. NO and $NO_2$ concentrations were monitored in real time by chemiluminescence with a detection limit of 0.5 ppb (model CLD 88Y, Eco Physics, MI) as were $O_3$ concentrations using an UV absorption spectroscopy with a detection limit of 0.5 ppb (model 49, Thermo Scientific, CO). In each experiment, the actual amounts of NO and $O_3$ injected were calculated using measured $NO_x$ and $O_3$ concentrations after steady state was reached (usually within 1 h). The wall loss rate of $NO_2$ was tested by monitoring $O_3$ (29 nmol $mol^{-1}$) and $NO_x$ (62 nmol $mol^{-1}$) over a 4-hour period. After the NO and $NO_2$ concentrations reached steady state, no decrease in $NO_2$ concentrations was observed showing that chamber wall loss was negligible.

Two sets of experiments were conducted to separately investigate the EIE, KIE and PHIFE. The first set of experiments was conducted in the dark. In each of these dark experiments, a range of NO and $O_3$ ($[O_3]<[NO]$) was injected into the chamber to produce NO-$NO_2$ mixtures with $[NO]/[NO_2]$ ratios ranging from 0.43 to 1.17. The N isotopes of these mixtures were used to investigate the EIE between NO and $NO_2$. The second set of experiments was conducted under

125 irradiation of UV lights (300-500 nm, see Appendix A for irradiation spectrum). Under such
126 conditions, NO, $NO_2$ and $O_3$ reached photochemical steady state, which combined the isotopic
127 effects of EIE, KIE and PHIFE. In addition, three experiments were conducted to measure the $\delta^{15}N$
128 value of the tank NO. In each of these experiments, a certain amount of $O_3$ was first injected into
129 the chamber, then approximately the same amount of NO was injected into the chamber to ensure
130 100% of the $NO_x$ was in the form of $NO_2$ with little $O_3$ (<3 nmol $mol^{-1}$) remaining in the chamber,
131 such that the $O_3$+$NO_2$ reaction was negligible. The $NO_2$ in the chamber was then collected and its
132 $\delta^{15}N$ value measured, which equates to the $\delta^{15}N$ value of the tank NO.

133 In all experiments, the concentrations of NO, $NO_2$ and $O_3$ were allowed to reach steady
134 state, and the product $NO_2$ was collected from the chamber using a honeycomb denuder tube. After
135 the NO, $NO_2$ and $O_3$ concentrations reached steady-state, well-mixed chamber air was drawn out
136 through a Norprene Thermoplastic tubing ~40 cm at 10 L $min^{-1}$ and passed through a honeycomb
137 denuder system (Chemcomb 3500, Thermo Scientific). Based on flow rate, the $NO_2$ residence time
138 in the was less than 0.5 second, thus in the light-on experiments where NO and $O_3$ coexisted, the
139 $NO_2$ produced inside the transfer tube through NO+$O_3$ reactions should be <0.03 ppb (using the
140 upper limit of NO and $O_3$ concentrations in our experiments). The honeycomb denuder system
141 consisted of two honeycomb denuder tubes connected in series. Each honeycomb denuder tube is
142 a glass cylinder of 38 mm long, 47 mm in diameter, and consist of 212 hexagonal tubes with inner
143 diameters of 2 mm. Before collecting samples, each denuder tube was coated with a solution of
144 10% KOH and 25% guaiacol in methanol and then dried by flowing $N_2$ gas through the denuder
145 tube for 15 seconds (Williams and Grosjean, 1990, Walters et al., 2016). The $NO_2$ reacted with
146 guaiacol coating and was converted into $NO_2^-$ that was retained on the denuder tube wall (Williams
147 and Grosjean, 1990). NO was inert to the denuder tube coating: a control experiment sampled pure

NO using the denuder tubes, which did not show any measurable $NO_2^-$. The $NO_2$ collection efficiency of a single honeycomb denuder tube was tested in another control experiment: air containing 66 nmol $mol^{-1}$ of $NO_2$ was drawn out of the chamber through a denuder tube, and the $NO_2$ concentration at the exit of the tube holder was measured and found to be below the detection limit (<1 nmol $mol^{-1}$), suggesting the collection efficiency was nearly 100% when [$NO_2$] <66 nmol $mol^{-1}$. Furthermore, when the denuder system consisted of two denuder tubes in series and $NO_2^-$ in the second denuder was below the detection limit indicating trivial $NO_2$ breakthrough. Each $NO_2$ collection lasted for 0.5-3 hours in order to collect enough $NO_2^-$ for isotopic analysis (~300 nmol). After collection, the $NO_2^-$ was leached from each denuder tube by rinsing thoroughly with 10 ml deionized water into a clean polypropylene container and stored frozen until isotopic analysis. Isotopic analysis was conducted at Purdue Stable Isotope Laboratory. For each sample, approximately 50 nmol of the $NO_2^-$ extract was mixed with 2 M sodium azide solution in acetic acid buffer in an air-tight glass vial, then shaken overnight to completely reduce all the $NO_2^-$ to $N_2O_{(g)}$ (Casciotti & McIlvin, 2007; McIlvin & Altabet, 2005). The product $N_2O$ was directed into a Thermo GasBench equipped with cryo-trap, then the $\delta^{15}N$ of the $N_2O$ was measured using a Delta-V Isotope Ratios Mass Spectrometer. Six coated denuders tubes that did not get exposed to $NO_2$ were also analyzed using the same chemical procedure, which did not show any measurable signal on the IRMS, suggesting the blank from both sampling process and the chemical conversion process was negligible. The overall analytical uncertainty for $\delta^{15}N$ analysis was 0.5 ‰ ($1\sigma$) based on replicate analysis of in house $NO_2^-$ standards.

## 3. Results and Discussions

### 3.1. Equilibrium Isotopic Fractionation between NO and $NO_2$

The equilibrium isotope fractionation factor, $\alpha(NO_2\text{-}NO)$, is the $^{15}N$ enrichment in $NO_2$ relative to NO, and is expressed as the ratio of rate constants $k_2$ / $k_1$ of two reactions:

$^{15}NO_2+^{14}NO \rightarrow ^{15}NO+^{14}NO_2$ R1, rate constant = $k_1$

$^{15}NO+^{14}NO_2 \rightarrow ^{15}NO_2+^{14}NO$ R2, rate constant = $k_2 = k_1\ \alpha(NO_2\text{-}NO)$

where $k_1$ is the rate constant of the isotopic exchange, which was previously determined to be $8.14\times10^{-14}$ $cm^3\ s^{-1}$ (Sharma et al., 1970). The reaction time required for NO-$NO_2$ to reach isotopic equilibrium was estimated using the exchange rate constants in a simple kinetics box model (BOXMOX, Knote et al., 2015). The model predicts that at typical $NO_x$ concentrations used during the chamber experiments (7.7-62.4 nmol $mol^{-1}$), isotopic equilibrium would be reached within 15 minutes (see Appendix B). Since the sample collection usually started 1 hour after $NO_x$ was well mixed in the chamber, there was sufficient time to reach full isotope equilibrium. The isotope equilibrium fractionation factor ($\alpha(NO_2\text{-}NO)$) is then calculated to be:

$$\alpha(NO_2 - NO) = \frac{[^{15}NO_2][^{14}NO]}{[^{14}NO_2][^{15}NO]} = \frac{R(NO_2)}{R(NO)} \quad \text{Eq. (1)}$$

where R(NO, $NO_2$) are the $^{15}N/^{14}N$ ratios of NO and $NO_2$. By definition, the $\delta^{15}N(NO)=(R(NO)/R(reference)-1)\times1000$ ‰ and $\delta^{15}N(NO_2)=(R(NO_2)/R(reference)-1)\times1000$ ‰, but hereafter, the $\delta^{15}N$ values of NO, $NO_2$ and $NO_x$ will be referred as $\delta(NO)$, $\delta(NO_2)$ and $\delta(NO_x)$, respectively. Eq. (1) leads to:

$$\delta(NO_2) - \delta(NO) = (\alpha(NO_2 - NO) - 1)\ (1 + \delta(NO)) \quad \text{Eq. (2)}$$

Using Eq. (2) and applying $NO_x$ isotopic mass balance ($\delta(NO_x)=f(NO_2)\delta(NO_2)+(1-f(NO_2))\delta(NO)$, $f(NO_2)=[NO_2]/([NO]+[NO_2])$ yields:

$$\frac{\delta(NO_2)-\delta(NO_x)}{1+\delta(NO_2)} = \frac{\alpha(NO_2-NO)-1}{\alpha(NO_2-NO)}\left(1 - f(NO_2)\right) \quad \text{Eq. (3)}$$

Here, $\delta(NO_x)$ equals to the $\delta^{15}N$ value of the cylinder NO and $f(NO_2)$ is the molar fraction of $NO_2$ with respect to total $NO_x$. Three experiments (see descriptions in method section) that measured $\delta(NO_x)$ showed consistent $\delta(NO_x)$ values of (-58.7±0.8) ‰ (n = 3), indicating $\delta(NO_x)$ remained unchanged throughout the experiments (as expected for isotope mass balance). Thus, the $\delta(NO_x)$ can be treated as a constant in Eq. (3), and the linear regression of $(\delta(NO_2)-\delta(NO_x))/(1+\delta(NO_2))$ versus $1-f(NO_2)$ should have an intercept of 0 and a slope of $(\alpha(NO_2\text{-}NO)-1)/\alpha(NO_2\text{-}NO)$.

The plot of $(\delta(NO_2)-\delta(NO_x))/(1+\delta(NO_2))$ as a function of $1-f(NO_2)$ values from five experiments yields an $\alpha(NO_2\text{-}NO)$ value of 1.0275±0.0012 at room temperature (Fig. 1B). This fractionation factor is comparable to previously measured values but with some differences. Our result agrees well with the $\alpha(NO_2\text{-}NO)$ value of 1.028±0.002 obtained by Begun and Melton (1956) at room temperature. However, Walters et al., (2016) determined the $\alpha(NO_2\text{-}NO)$ values of NO-$NO_2$ exchange in a 1-liter reaction vessel, which showed a slightly higher $\alpha(NO_2\text{-}NO)$ value of 1.035. This discrepancy might originate from rapid heterogeneous reactions on the wall of the reaction vessel at high $NO_x$ concentrations and the small chamber size used by Walters et al. (2016). They used a reaction vessel made of Pyrex, which is known to absorb water (Do Remus et al., 1983; Takei et al., 1997) that can react with $NO_2$ forming HONO, $HNO_3$ and other N compounds. Additionally, previous studies have suggested that Pyrex walls enhance the formation rate of $N_2O_4$ by over an order of magnitude (Barney & Finlayson-Pitts, 2000; Saliba et al., 2001), which at isotopic equilibrium is enriched in $^{15}N$ compared to NO and $NO_2$ (Walters & Michalski, 2015). Therefore, their measured $\alpha(NO_2\text{-}NO)$ might be slightly higher than the actual $\alpha(NO_2\text{-}NO)$ value. In this work, the 10 $m^3$ chamber has a much smaller surface to volume ratio relative to Walters et al. (2016) which minimizes wall effects, and the walls were made of Teflon that minimize $NO_2$ surface reactivity, which was evidenced by the $NO_2$ wall loss control experiment. Furthermore,

the low $NO_x$ mixing ratios in our experiments minimized $N_2O_4$ and $N_2O_3$ formation. At NO and $NO_2$ concentrations of 50 nmol $mol^{-1}$ the steady state concentrations of $N_2O_4$ and $N_2O_3$ were calculated to be 0.014 and 0.001 pmol $mol^{-1}$, respectively (Atkinson et al., 2004). Therefore, we suggest our measured $\alpha(NO_2\text{-}NO)$ value (1.0275±0.0012) may better reflect the room temperature (298 K) NO-$NO_2$ EIE in the ambient environment.

Unfortunately, the chamber temperature could not be controlled so we were not able to investigate the temperature dependence of the EIE. Hence, we speculate that the $\alpha(NO_2\text{-}NO)$ follows a similar temperature dependence pattern calculated in Walters et al. (2016). Walters et al. (2016) suggested that, the $\alpha(NO_2\text{-}NO)$ value would be 0.0047 higher at 273 K and 0.002 lower at 310 K, relative to room temperature (298 K). Using this pattern and our experimentally determined data, we suggest the $\alpha(NO_2\text{-}NO)$ values at 273 K, 298 K and 310 K are 1.0322±0.0012, 1.0275±0.0012 and 1.0255±0.0012, respectively. This 0.0067 variation at least partially contribute to the daily and seasonal variations of $\delta^{15}N$ values of $NO_2$ and nitrate in some areas (e.g., polar regions with strong seasonal temperature variation). Thus, future investigations should be conducted to verify the EIE temperature dependence.

### 3.2. Kinetic isotopic fractionation of Leighton Cycle

The photochemical reactions of $NO_x$ will compete with the isotope exchange fractionations between NO and $NO_2$. The NO-$NO_2$ photochemical cycle in the chamber was controlled by the Leighton cycle: $NO_2$ photolysis and the NO + $O_3$ reaction. This is because there were no VOCs in the chamber so no $RO_2$ was produced, which excludes the NO + $RO_2$ reaction. Likewise, the low water vapor content (RH<10%) and the minor flux of photons < 310 nm results in minimal OH production and hence little $HO_2$ formation and subsequently trivial amount of $NO_2$ would be

formed by NO + $HO_2$. Applying these limiting assumptions, the EIE between NO and $NO_2$ (R1-R2) were only competing with the KIE (R3-R4) and the PHIFE in R5-R6:

$^{14}NO_2 \rightarrow {}^{14}NO + O$ R3, rate constant=$j(NO_2)$

$^{15}NO_2 \rightarrow {}^{15}NO + O$ R4, rate constant=$j(NO_2)\ \alpha_1$

$^{14}NO + O_3 \rightarrow {}^{14}NO_2 + O_2$ R5, rate constant=$k_5$

$^{15}NO + O_3 \rightarrow {}^{15}NO_2 + O_2$ R6, rate constant=$k_5\ \alpha_2$

In which $j(NO_2)$ is the $NO_2$ photolysis rate ($1.4\times10^{-3}$ $s^{-1}$ in these experiments), $k_5$ is the rate constant for the $NO+O_3$ reaction ($1.73\times10^{-14}$ $cm^3$ $s^{-1}$, Atkinson et al., 2004), and $\alpha_{1,2}$ are isotopic fractionation factors for the two reactions. Previous studies (Freyer et al., 1993; Walters et al., 2016) have attempted to assess the competition between EIE (R1-R2), KIE and PHIFE (R3-R6), but none of them quantified the relative importance of the two processes, nor were $\alpha_1$ or $\alpha_2$ values experimentally determined. Here we provide the mathematical solution of EIE, KIE and PHIFE to illustrate how R1-R6 affect the isotopic fractionations between NO and $NO_2$.

First, the $NO_2$ lifetime with respect to isotopic exchange with NO ($\tau_{exchange}$) and photolysis ($\tau_{photo}$) was determined:

$$\tau_{exchange} = \frac{1}{k_1\,[NO]} \quad \text{Eq. (4)}$$

$$\tau_{photo} = \frac{1}{j(NO_2)} \quad \text{Eq. (5)}$$

We then define an A factor:

$$A = \begin{cases} \frac{\tau_{exchange}}{\tau_{photo}} & \text{when } j(NO_2) \neq 0 \\ 0 & \text{when } j(NO_2) = 0 \end{cases} \quad \text{Eq. (6)}$$

Using R1-R6 and Eq. (1)-(6), we solved steady-state $\delta(NO_2)$ and $\delta(NO)$ values (see calculations in Appendix C). Our calculations show that the $\delta(NO_2)$-$\delta(NO)$ and $\delta(NO_2)$-$\delta(NO_x)$ values at steady state can be expressed as functions of $\alpha_1$, $\alpha_2$, $\alpha(NO_2\text{-}NO)$ and A:

$$\delta(NO_2) - \delta(NO) = \frac{(\alpha_2-\alpha_1)\,A+(\alpha(NO_2-NO)-1)}{A+1}(1+\delta(NO)) \quad \text{Eq. (7)}$$

$$\delta(NO_2) - \delta(NO_x) = \frac{(\alpha_2-\alpha_1)\,A+(\alpha(NO_2-NO)-1)}{A+1}(1+\delta(NO))(1-f(NO_2)) \quad \text{Eq. (8)}$$

Equation (7) shows the isotopic fractionation between NO and $NO_2$ ($\delta(NO_2)$-$\delta(NO)$) is determined by A, the EIE factor ($\alpha(NO_2\text{-}NO)$-1) and the ($\alpha_2$-$\alpha_1$) factor assuming (1+$\delta(NO)$) is close to 1. This ($\alpha_2$-$\alpha_1$) represents a combination of KIE and PHIFE, suggesting they act together as one factor; therefore, we name the ($\alpha_2$-$\alpha_1$) factor Leighton Cycle Isotopic Effect, i.e., LCIE. Using measured ($\delta(NO_2)$-$\delta(NO)$)/(1+$\delta(NO)$) values, A values, and the previously determined EIE factor, we calculated that the best fit for the LCIE factor was (-10±5) ‰ (showing the lowest Rooted Mean Square Error, RMSE, of 1.1‰, Fig. 1C). The uncertainties in the LCIE factor are relatively higher than that of the EIE factor, mainly because of the accumulated analytical uncertainties at low $NO_x$ and $O_3$ concentrations, and low A values (0.10-0.28) due to the relatively low $j(NO_2)$ value ($1.4\times10^{-3}$ $s^{-1}$) under the chamber irradiation conditions.

This LCIE factor determined in our experiments is in good agreement with theoretical calculations. Walters and Michalski (2016) previously used an *ab initio* approach to determine an $\alpha_2$ value of 0.9933 at room temperature, 0.9943 at 237 K and 0.9929 at 310 K. The total variation of $\alpha_2$ values from 273 K to 310 K is only 1.4 ‰, significantly smaller than our experimental uncertainty (±5 ‰). The $\alpha_1$ value was calculated using a ZPE shift model (Miller & Yung, 2000) to calculate the isotopic fractionation of $NO_2$ by photolysis. Briefly, this model assumes both isotopologues have the same quantum yield function and the PHIFE was only caused by the differences in the $^{15}NO_2$ and $^{14}NO_2$ absorption cross-section as a function of wavelength, thus $\alpha_1$

values do not vary by temperature. The $^{15}NO_2$ absorption cross-section was calculated by shifting the $^{14}NO_2$ absorption cross-section by the $^{15}NO_2$ zero-point energy (Michalski et al., 2004). When the ZPE shift model was used with the irradiation spectrum of the chamber lights, the resulting $\alpha_1$ value was 1.0023. Therefore, the theoretically predicted $\alpha_2$-$\alpha_1$ value should be -0.0090, i.e., (-9.0±0.7) ‰ when temperature ranges from 273 K to 310 K. This result shows excellent agreement with our experimentally determined room temperature $\alpha_2$-$\alpha_1$ value of (-10±5) ‰.

This model was then used to evaluate the variations of $\alpha_1$ value to different lighting conditions. The TUV model (TUV5.3.2, Madronich & Flocke, 1999) was used to calculate the solar wavelength spectrum at three different conditions: early morning/late afternoon (solar zenith angle=85 degree), mid-morning/afternoon (solar zenith angle=45 degree), noon (solar zenith angle=0 degree). These spectrums were used in the ZPE shift model to calculate the $\alpha_1$ values, which are 1.0025, 1.0028, and 1.0029 at solar zenith angles of 85, 45 and 0 degree, respectively. These values, along with the predicted $\alpha_1$ value in the chamber, showed a total span of 0.6‰ (1.0026±0.0003), which is again significantly smaller than our measured uncertainty. Therefore, we suggest that our experimentally determined LCIE factor ((-10±5) ‰) can be used in most tropospheric solar irradiation spectrums.

The equations can also be applied in tropospheric environments to calculate the combined isotopic fractionations of EIE and LCIE for NO and $NO_2$. First, the $NO_2$ sink reactions (mainly $NO_2$+OH in the daytime) are at least 2-3 orders of magnitude slower than the Leighton cycle and the NO-$NO_2$ isotope exchange reactions (Walters et al., 2016), therefore their effects on the $\delta(NO_2)$ should be minor. Second, although the conversion of NO into $NO_2$ in the ambient environment is also controlled by NO + $RO_2$ and $HO_2$ in addition to NO+$O_3$ (e.g., King et al., 2001), Eq. (7) still showed good agreement with field observations in previous studies. Freyer et al. (1993)

303 determined the annual average daytime $\delta(NO_2)$-$\delta(NO)$ at Julich, Germany along with average
304 daytime NO concentration (9 nmol $mol^{-1}$, similar to our experimental conditions) to be
305 (+18.03±0.98) ‰. Using Eq. (7), assuming the daytime average $j(NO_2)$ value throughout the year
306 was $(5.0\pm1.0)\times10^{-3}$, and a calculated A value from measured $NO_x$ concentration ranged from 0.22-
307 0.33, the average NO-$NO_2$ fractionation factor was calculated to be (+18.8±1.4) ‰ (Fig. 1C), in
308 excellent agreement with the measurements in the present study. This agreement suggests the
309 NO+$RO_2$/$HO_2$ reactions might have similar fractionation factors as NO+$O_3$. Therefore, we suggest
310 Eq. (7) and (8) can be used to estimate the isotopic fractionations between NO and $NO_2$ in the
311 troposphere.
312
313 **3.3 Calculating nitrogen isotopic fractionations of NO-$NO_2$**
314 First, Eq. (7) was used to calculate the $\Delta(NO_2\text{-}NO) = \delta(NO_2)\text{-}\delta(NO)$ at a wide range of
315 $NO_x$ concentrations, $f(NO_2)$ and $j(NO_2)$ values (Fig. 2A-D), assuming $(1+\delta(NO))=1$. $j(NO_2)$
316 values of 0 $s^{-1}$ (Fig. 2A), $1.4\times10^{-3}$ $s^{-1}$ (Fig. 2B), $5\times10^{-3}$ $s^{-1}$ (Fig. 2C) and $1\times10^{-2}$ $s^{-1}$ (Fig. 2D) were
317 selected to represent nighttime, dawn (as well as the laboratory conditions of our experiments),
318 daytime average and noon, respectively. Each panel represented a fixed $j(NO_2)$ value, and the
319 $\Delta(NO_2\text{-}NO)$ values were calculated as a function of the A value, which was derived from $NO_x$
320 concentration and $f(NO_2)$. The A values have a large span, from 0 to 500, depending on the $j(NO_2)$
321 value and the NO concentration. When A=0 ($j(NO_2)=0$) and $f(NO_2)<1$ (meaning NO-$NO_2$ coexist
322 and $[O_3]=0$), Eq. (7) and (8) become Eq. (2) and (3), showing the EIE was the sole factor, the
323 $\Delta(NO_2\text{-}NO)$ values were solely controlled by EIE which has a constant value of +27.5 ‰ at 298K
324 (Fig. 2A). When $j(NO_2)>0$, the calculated $\Delta(NO_2\text{-}NO)$ values showed a wide range from -10.0 ‰
325 (controlled by LCIE factor: $\alpha_2\text{-}\alpha_1$=-10 ‰) to +27.5 ‰ (controlled by EIE factor: $\alpha(NO_2\text{-}NO)\text{-}1$ =

+27.5 ‰). Fig. 2B-D display the transition from a LCIE-dominated regime to an EIE-dominated regime. The LCIE-dominated regime is characterized by low [$NO_x$] (<50 pmol $mol^{-1}$), representing remote ocean areas and polar regions (Beine et al., 2002; Custard et al., 2015). At this range the A value can be greater than 200, thus Eq. (7) can be simplified as: $\Delta(NO_2\text{-}NO) = \alpha_2\text{-}\alpha_1$, suggesting the LCIE almost exclusively controls the NO-$NO_2$ isotopic fractionation. The $\Delta(NO_2\text{-}NO)$ values of these regions are predicted to be <0 ‰ during most time of the day and < -5 ‰ at noon. On the other hand, the EIE-dominated regime was characterized by high [$NO_x$] (>20 nmol $mol^{-1}$) and low $f(NO_2)$ (< 0.6), representative of regions with intensive NO emissions, e.g., near roadside or stack plumes (Clapp & Jenkin, 2001; Kimbrough et al., 2017). In this case, the $\tau_{exchange}$ are relatively short (10-50 s) compared to the $\tau_{photo}$ (approximately 100 s at noon and 1000 s at dawn), therefore the A values are small (0.01-0.5). The EIE factor in this regime thus is much more important than the LCIE factor, resulting in high $\Delta(NO_2\text{-}NO)$ values (>20 ‰). Between the two regimes, both EIE and LCIE are competitive and therefore it is necessary to use Eq. (7) to quantify the $\Delta(NO_2\text{-}NO)$ values.

Fig. 2 also implies that changes in the $j(NO_2)$ value can cause the diurnal variations in $\Delta(NO_2\text{-}NO)$ values. Changing $j(NO_2)$ would affect the value of A and consequently the NO-$NO_2$ isotopic fractionations in two ways: 1) changes in $j(NO_2)$ value would change the photolysis intensity, therefore the $\tau_{photo}$ value; 2) in addition, changes in $j(NO_2)$ value would also alter the steady state NO concentration, therefore changing the $\tau_{exchange}$ (Fig. 2C). The combined effect of these two factors on the A value varies along with the atmospheric conditions, and thus needs to be carefully calculated using $NO_x$ concentration data and atmospheric chemistry models.

We then calculated the differences of $\delta^{15}N$ values between $NO_2$ and total $NO_x$, e.g. $\Delta(NO_2\text{-}NO_x) = \delta(NO_2)\text{-}\delta(NO_x)$ in Fig. 2E-H. Since $\Delta(NO_2\text{-}NO_x)$ are connected through the observed $\delta^{15}N$

of $NO_2$ (or nitrate) to the $\delta^{15}N$ of $NO_x$ sources, this term might be useful in field studies (e.g., Chang et al., 2018; Zong et al., 2017). The calculated $\Delta(NO_2\text{-}NO_x)$ values (Fig. 2E-H) also showed a LCIE-dominated regime at low [$NO_x$] and an EIE-dominated regime at high [$NO_x$]. The $\Delta(NO_2\text{-}NO_x)$ values were dampened by the $1\text{-}f(NO_2)$ factor comparing to $\Delta(NO_2\text{-NO})$, as shown in Eq. (3) and (8): $\Delta(NO_2\text{-}NO_x) = \Delta(NO_2\text{-NO})\ (1\text{-}f(NO_2))$. At high $f(NO_2)$ values (>0.8), the differences between $\delta(NO_2)$ and $\delta(NO_x)$ were less than 5 ‰, thus the measured $\delta(NO_2)$ values were similar to $\delta(NO_x)$, although the isotopic fractionation between NO and $NO_2$ could be noteworthy. Some ambient environments with significant NO emissions or high $NO_2$ photolysis rates usually have $f(NO_2)$ values between 0.4-0.8 (Mazzeo et al., 2005; Vicars et al., 2013). In this scenario, the $\Delta(NO_2\text{-}NO_x)$ values in Fig. 2F-H showed wide ranges of -4.8 ‰ to +15.6 ‰, -6.0 ‰ to +15.0 ‰, and -6.3 ‰ to +14.2 ‰ at $j(NO_2)$=$1.4\times10^{-3}$ $s^{-1}$, $5\times10^{-3}$ $s^{-1}$, $1\times10^{-2}$ $s^{-1}$, respectively. These significant differences again highlighted the importance of both LCIE and EIE (Eq. (7) and (8)) in calculating the $\Delta(NO_2\text{-}NO_x)$. In the following discussion, we assume 1) the $\alpha_1$ value remain constant (see discussion above), 2) the $NO+RO_2/HO_2$ reactions have the same fractionation factors ($\alpha_2$) as $NO+O_3$, and 3) both EIE and LCIE do not display significant temperature dependence, then use Equations (7) and (8) and this laboratory determined LCIE factor (-10 ‰) to calculate the nitrogen isotopic fractionation between NO and $NO_2$ at various tropospheric atmospheric conditions.

## 4. Implications

The daily variations of $\Delta(NO_2\text{-}NO_x)$ values at two roadside $NO_x$ monitoring sites were predicted to demonstrate the effects of $NO_x$ concentrations to the $NO\text{-}NO_2$ isotopic fractionations. Hourly NO and $NO_2$ concentrations were acquired from a roadside site at Anaheim, CA (https://www.arb.ca.gov) and an urban site at Evansville, IN (http://idem.tx.sutron.com) on July

25, 2018. The hourly $j(NO_2)$ values output from the TUV model (Madronich & Flocke, 1999) at these locations was used to calculate the daily variations of $\Delta(NO_2\text{-}NO_x)$ values (Fig. 3A, B) by applying Eq. (8) and assuming $(1+\delta(NO))=1$. Hourly $NO_x$ concentrations were 12-51 nmol $mol^{-1}$ at Anaheim and 9-38 nmol $mol^{-1}$ at Evansville and the $f(NO_2)$ values at both sites did not show significant daily variations (0.45±0.07 at Anaheim and 0.65±0.08 at Evansville), likely because the $NO_x$ concentrations were controlled by the high NO emissions from the road (Gao, 2007). The calculated $\Delta(NO_2\text{-}NO_x)$ values using Eq. (8) showed significant diurnal variations. During the nighttime, the isotopic fractionations were solely controlled by the EIE, the predicted $\Delta(NO_2\text{-}NO_x)$ values were (+14.5±2.0) ‰ and (+8.7±2.1) ‰ at Anaheim and Evansville, respectively. During the daytime, the existence of LCIE lowered the predicted $\Delta(NO_2\text{-}NO_x)$ values to (+9.8±1.7) ‰ at Anaheim and (+3.1±1.5) ‰ at Evansville while the $f(NO_2)$ values at both sites remained similar. The lowest $\Delta(NO_2\text{-}NO_x)$ values for both sites (+7.0 ‰ and +1.7 ‰) occurred around noon when the $NO_x$ photolysis was the most intense. In contrast, if one neglects the LCIE factor in the daytime, the $\Delta(NO_2\text{-}NO_x)$ values would be (+12.9±1.5) ‰ and (+10.0±1.6) ‰ respectively, an overestimation of 3.1 ‰ and 6.9 ‰. These discrepancies suggested that the LCIE played an important role in the NO-$NO_2$ isotopic fractionations and neglecting it could bias the $NO_x$ source apportionment using $\delta^{15}N$ of $NO_2$ or nitrate.

The role of LCIE was more important in less polluted sites. The $\Delta(NO_2\text{-}NO_x)$ values calculated for a suburban site near San Diego, CA, USA, again using the hourly $NO_x$ concentrations (https://www.arb.ca.gov, Fig. 3C) and $j(NO_2)$ values calculated from the TUV model. $NO_x$ concentrations at this site varied from 1 to 9 nmol $mol^{-1}$ and assuming $(1+\delta(NO))=1$. During the nighttime, $NO_x$ was in the form of $NO_2$ ($f(NO_2) = 1$) because $O_3$ concentrations were higher than $NO_x$, thus the $\delta(NO_2)$ values should be identical to $\delta(NO_x)$ ($\Delta(NO_2\text{-}NO_x) = 0$). In the

daytime a certain amount of NO was produced by direct NO emission and $NO_2$ photolysis but the $f(NO_2)$ was still high (0.73±0.08). Our calculation suggested the daytime $\Delta(NO_2\text{-}NO_x)$ values should be only (+1.3±3.2) ‰ with a lowest value of -1.3 ‰. These $\Delta(NO_2\text{-}NO_x)$ values were similar to the observed and modeled summer daytime $\delta(NO_2)$ values in West Lafayette, IN (Walters et al., 2018), which suggest the average daytime $\Delta(NO_2\text{-}NO_x)$ values at $NO_x$ = (3.9±1.2) nmol $mol^{-1}$ should range from +0.1 ‰ to +2.4 ‰. In this regime, we suggest the $\Delta(NO_2\text{-}NO_x)$ values were generally small due to the significant contribution of LCIE and high $f(NO_2)$.

The LCIE should be the dominant factor controlling the NO-$NO_2$ isotopic fractionation at remote regions, resulting in a completely different diurnal pattern of $\Delta(NO_2\text{-}NO_x)$ compared with the urban-suburban area. Direct hourly measurements of $NO_x$ at remote sites are rare, thus we used total $NO_x$ concentration of 50 pmol $mol^{-1}$, daily $O_3$ concentration of 20 nmol $mol^{-1}$ at Summit, Greenland (Dibb et al., 2002; Hastings et al., 2004; Honrath et al., 1999; Yang et al., 2002), and assumed $(1+\delta(NO))=1$ and the conversion of NO to $NO_2$ was completely controlled by $O_3$ to calculate the $NO/NO_2$ ratios. Here the isotopes of $NO_x$ were almost exclusively controlled by the LCIE due to the high A values (>110). The $\Delta(NO_2\text{-}NO_x)$ values displayed a clear diurnal pattern (Fig. 3D) with highest value of -0.3 ‰ in the "nighttime" (solar zenith angle >85 degree) and lowest value of -5.0 ‰ in the mid-day. This suggest that the isotopic fractionations between NO and $NO_2$ were almost completely controlled by LCIE at remote regions, when $NO_x$ concentrations were <0.1 nmol $mol^{-1}$. However, since the isotopic fractionation factors of nitrate-formation reactions ($NO_2$+OH, $NO_3$+HC, $N_2O_5+H_2O$) are still unknown, more studies are needed to fully explain the daily and seasonal variations of $\delta(NO_3^-)$ at remote regions.

Nevertheless, our results have a few limitations. First, currently there are very few field observations that can be used to evaluate our model, therefore, future field observations that

418 measure the $\delta^{15}N$ values of ambient NO and $NO_2$ should be carried out to test our model. Second,
419 more work, including theoretical and experimental studies, is needed to investigate the isotope
420 fractionation factors occurring during the conversion from $NO_x$ to $NO_y$ and nitrate: in the $NO_y$
421 cycle, EIE (isotopic exchange between $NO_2$, $NO_3$ and $N_2O_5$), KIE (formation of $NO_3$, $N_2O_5$ and
422 nitrate) and PHIFE (photolysis of $NO_3$, $N_2O_5$, HONO and sometimes nitrate) may also exist and
423 be relevant for the $\delta^{15}N$ of $HNO_3$ and HONO. In particular, the N isotope fractionation occurring
424 during the $NO_2 + OH \rightarrow HNO_3$ reaction needs investigation. Such studies could help us modeling
425 the isotopic fractionation between $NO_x$ emission and nitrate, and eventually enable us to analyze
426 the $\delta^{15}N$ value of $NO_x$ emission by measuring the $\delta^{15}N$ values of nitrate aerosols and nitrate in wet
427 depositions. Third, our discussion only focuses on the reactive nitrogen chemistry in the
428 troposphere, however, the nitrogen chemistry in the stratosphere is drastically different from the
429 tropospheric chemistry, thus future studies are also needed to investigate the isotopic fractionations
430 in the stratospheric nitrogen chemistry. Last, the temperature dependence of both EIE and LCIE
431 needs to be carefully investigated, because of the wide range of temperature in both troposphere
432 and stratosphere. Changes in temperature could alter the isotopic fractionation factors of both EIE
433 and LCIE, as well as contribute to the seasonality of isotopic fractionations between $NO_x$ and $NO_y$
434 molecules.
435
436 **5. Conclusions**
437 The effect of $NO_x$ photochemistry on the nitrogen isotopic fractionations between NO and
438 $NO_2$ was investigated. We first measured the isotopic fractionations between NO and $NO_2$ and
439 provided mathematical solutions to assess the impact of $NO_x$ level and $NO_2$ photolysis rate ($j(NO_2)$)
440 to the relative importance of EIE and LCIE. The EIE and LCIE isotope fractionation factors, at

441 room temperature, were determined to be 1.0275±0.0012 and 0.990±0.005, respectively. These
442 calculations and measurements can be used to determine the steady state $\Delta(NO_2\text{-}NO)$ and $\Delta(NO_2\text{-}NO_x)$ values at room temperature. Subsequently we applied our equations to polluted, clean and
444 remote sites to model the daily variations of $\Delta(NO_2\text{-}NO_x)$ values. We found that the $\Delta(NO_2\text{-}NO_x)$
445 values could vary from over +20 ‰ to less than -5 ‰ depending on the environment: in general,
446 the role of LCIE becoming more important at low $NO_x$ concentrations, which tend to decrease the
447 $\Delta(NO_2\text{-}NO_x)$ values. Our work provided a mathematical approach to quantify the nitrogen isotopic
448 fractionations between NO and $NO_2$ that can be applied to many tropospheric environments, which
449 could help interpret the measured $\delta^{15}N$ values of $NO_2$ and nitrate in field observation studies.
450

451 **Acknowledgement**

452 We thank NCAR's Advanced Study Program granted to Jianghanyang Li. The National
453 Center for Atmospheric Research is operated by the University Corporation for Atmospheric
454 Research, under the sponsorship of the National Science Foundation. We also thank funding
455 support from Purdue Climate Change Research Center and A. H. Ismail Interdisciplinary Program
456 Doctoral Research Travel Award granted by Purdue University.

457 **Data Availability**

458 Data acquired from this study was deposited at Open Sciences Framework (Li, 2019,
459 DOI 10.17605/OSF.IO/JW8HU).

460 **Author contribution**

461 J. Li and G. Michalski designed the experiments, X. Zhang and J. Li conducted the
462 experiments. X. Zhang, G. Michalski, J. Orlando and G. Tyndall helped J. Li in interpreting the

results. The manuscript was written by J. Li and all the authors have contributed during the revision of this manuscript.

**Competing interest**

The authors declare no competing interest.

**References:**


Atkinson, R., Baulch, D. L., Cox, R. A., Crowley, J. N., Hampson, R. F., Hynes, R. G., Jenkin, M. E., Rossi, M. J., and Troe, J. (2004). Evaluated kinetic and photochemical data for atmospheric chemistry: Volume I-gas phase reactions of $O_x$, $HO_x$, $NO_x$ and $SO_x$. Atmospheric chemistry and physics, 4(6), 1461-1738. https://doi.org/10.5194/acp-4-1461-2004, 2004.

Barney, W. S., & Finlayson-Pitts, B. J. (2000). Enhancement of $N_2O_4$ on porous glass at room temperature: A key intermediate in the heterogeneous hydrolysis of $NO_2$? The Journal of Physical Chemistry A, 104(2), 171–175. https://doi.org/10.1021/jp993169b

Begun, G. M., & Fletcher, W. H. (1960). Partition function ratios for molecules containing nitrogen isotopes. The Journal of Chemical Physics, 33(4), 1083–1085. https://doi.org/10.1063/1.1731338

Begun, G. M., & Melton, C. E. (1956). Nitrogen isotopic fractionation between NO and $NO_2$ and mass discrimination in mass analysis of $NO_2$. The Journal of Chemical Physics, 25(6), 1292–1293. https://doi.org/10.1063/1.1743215

Beine, H. J., Honrath, R. E., Dominé, F., Simpson, W. R., & Fuentes, J. D. (2002). $NO_x$ during background and ozone depletion periods at Alert: Fluxes above the snow surface. Journal of Geophysical Research: Atmospheres, 107(D21), ACH-7. https://doi.org/10.1029/2002JD002082

Bigeleisen, J., & Mayer, M. G. (1947). Calculation of equilibrium constants for isotopic exchange reactions. The Journal of Chemical Physics, 15(5), 261-267. https://doi.org/10.1063/1.1746492

Bigeleisen, J., & Wolfsberg, M. (1957). Theoretical and experimental aspects of isotope effects in chemical kinetics. Advances in Chemical Physics, 15–76. https://doi.org/10.1002/9780470143476.ch2

Casciotti, K. L., & McIlvin, M. R. (2007). Isotopic analyses of nitrate and nitrite from reference mixtures and application to Eastern Tropical North Pacific waters. Marine Chemistry, 107(2), 184–201. https://doi.org/10.1016/j.marchem.2007.06.021

Chang, Y., Zhang, Y., Tian, C., Zhang, S., Ma, X., Cao, F., et al. (2018). Nitrogen isotope fractionation during gas-to-particle conversion of $NO_x$ to $NO_3^-$ in the atmosphere–implications for

isotope-based $NO_x$ source apportionment. Atmospheric Chemistry and Physics, 18(16), 11647–11661. https://doi.org/10.5194/acp-18-11647-2018, 2018.

Clapp, L. J., & Jenkin, M. E. (2001). Analysis of the relationship between ambient levels of $O_3$, $NO_2$ and NO as a function of $NO_x$ in the UK. Atmospheric Environment, 35(36), 6391–6405. https://doi.org/10.1016/S1352-2310(01)00378-8

Custard, K. D., Thompson, C. R., Pratt, K. A., Shepson, P. B., Liao, J., Huey, L. G., Orlando, J. J., Weinheimer, A. J., Apel, E., Hall, S. R., Flocke, F., Mauldin, L., Hornbrook, R. S., Pöhler, D., General, S., Zielcke, J., Simpson, W. R., Platt, U., Fried, A., Weibring, P., Sive, B. C., Ullmann, K., Cantrell, C., Knapp, D. J., and Montzka, D. D.: The NOx dependence of bromine chemistry in the Arctic atmospheric boundary layer, Atmos. Chem. Phys., 15, 10799–10809, https://doi.org/10.5194/acp-15-10799-2015, 2015.

Dibb, J. E., Arsenault, M., Peterson, M. C., & Honrath, R. E. (2002). Fast nitrogen oxide photochemistry in Summit, Greenland snow. Atmospheric Environment, 36(15–16), 2501–2511. https://doi.org/10.1016/S1352-2310(02)00130-9

Do Remus, R. H., Mehrotra, Y., Lanford, W. A., & Burman, C. (1983). Reaction of water with glass: influence of a transformed surface layer. Journal of Materials Science, 18(2), 612–622. https://doi.org/10.1007/BF00560651

Elliott, E. M., Kendall, C., Boyer, E. W., Burns, D. A., Lear, G. G., Golden, H. E., Harlin, K., Bytnerowicz, A., Butler, T. J., and Glatz, R. ( 2009). Dual nitrate isotopes in dry deposition: Utility for partitioning $NO_x$ source contributions to landscape nitrogen deposition. Journal of Geophysical Research: Biogeosciences, 114(G4), G04020. https://doi.org/10.1029/2008JG000889

Felix, J. D., & Elliott, E. M. (2014). Isotopic composition of passively collected nitrogen dioxide emissions: Vehicle, soil and livestock source signatures. Atmospheric Environment, 92, 359–366. https://doi.org/10.1016/j.atmosenv.2014.04.005

Felix, J. D., Elliott, E. M., & Shaw, S. L. (2012). Nitrogen isotopic composition of coal-fired power plant $NO_x$: influence of emission controls and implications for global emission inventories. Environmental Science & Technology, 46(6), 3528–3535. https://doi.org/10.1021/es203355v

Frey, M. M., Savarino, J., Morin, S., Erbland, J., & Martins, J. M. F. (2009). Photolysis imprint in the nitrate stable isotope signal in snow and atmosphere of East Antarctica and implications for reactive nitrogen cycling. Atmos. Chem. Phys, 9, 8681-8696. https://doi.org/10.5194/acp-9-8681-2009, 2009.

Freyer, H. D. (1991). Seasonal variation of $^{15}N/^{14}N$ ratios in atmospheric nitrate species. Tellus B, 43(1), 30–44. https://doi.org/10.1034/j.1600-0889.1991.00003.x

Freyer, H. D., Kley, D., Volz-Thomas, A., & Kobel, K. (1993). On the interaction of isotopic exchange processes with photochemical reactions in atmospheric oxides of nitrogen. Journal of Geophysical Research: Atmospheres, 98(D8), 14791–14796. https://doi.org/10.1029/93JD00874

Gao, H. O. (2007). Day of week effects on diurnal ozone/$NO_x$ cycles and transportation emissions in Southern California. Transportation Research Part D: Transport and Environment, 12(4), 292–305. https://doi.org/10.1016/j.trd.2007.03.004

Gobel, A. R., Altieri, K. E., Peters, A. J., Hastings, M. G., & Sigman, D. M. (2013). Insights into anthropogenic nitrogen deposition to the North Atlantic investigated using the isotopic composition of aerosol and rainwater nitrate. Geophysical Research Letters, 40(22), 5977–5982. https://doi.org/10.1002/2013GL058167

Hastings, M G, Jarvis, J. C., & Steig, E. J. (2009). Anthropogenic impacts on nitrogen isotopes of ice-core nitrate. Science, 324(5932), 1288. DOI: 10.1126/science.1170510

Hastings, M G, Steig, E. J., & Sigman, D. M. (2004). Seasonal variations in N and O isotopes of nitrate in snow at Summit, Greenland: Implications for the study of nitrate in snow and ice cores. Journal of Geophysical Research: Atmospheres, 109(D20). https://doi.org/10.1029/2004JD004991

Honrath, R. E., Peterson, M. C., Guo, S., Dibb, J. E., Shepson, P. B., & Campbell, B. (1999). Evidence of $NO_x$ production within or upon ice particles in the Greenland snowpack. Geophysical Research Letters, 26(6), 695–698. https://doi.org/10.1029/1999GL900077

Jarvis, J. C., Steig, E. J., Hastings, M. G., & Kunasek, S. A. (2008). Influence of local photochemistry on isotopes of nitrate in Greenland snow. Geophysical Research Letters, 35(21). https://doi.org/10.1029/2008GL035551

Kendall, C., Elliott, E. M., & Wankel, S. D. (2007). Tracing anthropogenic inputs of nitrogen to ecosystems. Stable Isotopes in Ecology and Environmental Science, 2, 375–449. https://doi.org/10.1002/9780470691854.ch12

Kimbrough, S., Owen, R. C., Snyder, M., & Richmond-Bryant, J. (2017). NO to $NO_2$ conversion rate analysis and implications for dispersion model chemistry methods using Las Vegas, Nevada near-road field measurements. Atmospheric Environment, 165, 23–34. https://doi.org/10.1016/j.atmosenv.2017.06.027

King, M. D., Canosa-Mas, C. E. and Wayne R. P. (2001). Gas-phase reactions between $RO_2$ and NO, $HO_2$ or $CH_3O_2$: correlations between rate constants and the SOMO energy of the peroxy ($RO_2$) radical. Atmospheric Environment 35.12 (2001): 2081-2088. https://doi.org/10.1016/S1352-2310(00)00501-X

Knote, C., Tuccella, P., Curci, G., Emmons, L., Orlando, J. J. Madronich, S., Baró, R., Jiménez-Guerrero, P., Luecken, D., Hogrefe, C., Forkel, R., Werhahn, J., Hirtl, M., Pérez, J. L., San José, R., Giordano, L., Brunner, D., Yahya, K., Zhang, Y., Influence of the choice of gas-phase mechanism on predictions of key gaseous pollutants during the AQMEII phase-2 intercomparison. Atmospheric Environment 115 (2015): 553-568. https://doi.org/10.1016/j.atmosenv.2014.11.066.

Li, J. (2019). Quantifying the nitrogen equilibrium and photochemistry-induced kinetic isotopic effects between NO and $NO_2$. Retrieved from osf.io/jw8hu

Madronich, S., & Flocke, S. (1999). The role of solar radiation in atmospheric chemistry. In Environmental photochemistry (pp. 1–26). The Handbook of Environmental Chemistry (Reactions and Processes), vol 2 / 2L. Springer, Berlin, Heidelberg. https://doi.org/10.1007/978-3-540-69044-3_1

Mazzeo, N. A., Venegas, L. E., & Choren, H. (2005). Analysis of NO, $NO_2$, $O_3$ and $NO_x$ concentrations measured at a green area of Buenos Aires City during wintertime. Atmospheric Environment, 39(17), 3055–3068. https://doi.org/10.1016/j.atmosenv.2005.01.029

McIlvin, M. R., & Altabet, M. A. (2005). Chemical conversion of nitrate and nitrite to nitrous oxide for nitrogen and oxygen isotopic analysis in freshwater and seawater. Analytical Chemistry, 77(17), 5589–5595. https://doi.org/10.1021/ac050528s

Michalski, G., Jost, R., Sugny, D., Joyeux, M., & Thiemens, M. (2004). Dissociation energies of six $NO_2$ isotopologues by laser induced fluorescence spectroscopy and zero-point energy of some triatomic molecules. The Journal of Chemical Physics, 121(15), 7153–7161. https://doi.org/10.1063/1.1792233

Michalski, G., Bockheim, J. G., Kendall, C., & Thiemens, M. (2005). Isotopic composition of Antarctic Dry Valley nitrate: Implications for $NO_y$ sources and cycling in Antarctica. Geophysical Research Letters, 32(13). https://doi.org/10.1029/2004GL022121

Miller, C. E., & Yung, Y. L. (2000). Photo-induced isotopic fractionation. Journal of Geophysical Research: Atmospheres, 105(D23), 29039–29051. https://doi.org/10.1029/2000JD900388

Monse, E. U., Spindel, W., & Stern, M. J. (1969). Analysis of isotope-effect calculations illustrated with exchange equilibria among oxynitrogen compounds. Rutgers-The State Univ., Newark, NJ. DOI: 10.1021/ba-1969-0089.ch009

Morin, S., Savarino, J., Frey, M. M., Domine, F., Jacobi, H.-W., Kaleschke, L., & Martins, J. M. F. (2009). Comprehensive isotopic composition of atmospheric nitrate in the Atlantic Ocean boundary layer from 65°S to 79°N. J. Geophys. Res, 114. https://doi.org/10.1029/2008JD010696

Park, Y.-M., Park, K.-S., Kim, H., Yu, S.-M., Noh, S., Kim, M.-S., Kim, J.-Y., Ahn, J.-Y., Lee, M.-D., Seok, K.-S., Kin, Y.-H., (2018). Characterizing isotopic compositions of TC-C, $NO_3^-$-N, and $NH_4^+$-N in PM2.5 in South Korea: Impact of China's winter heating. https://doi.org/10.1016/j.envpol.2017.10.072

Saliba, N. A., Yang, H., & Finlayson-Pitts, B. J. (2001). Reaction of gaseous nitric oxide with nitric acid on silica surfaces in the presence of water at room temperature. The Journal of Physical Chemistry A, 105(45), 10339–10346. https://doi.org/10.1021/jp012330r

Savarino, J., Morin, S., Erbland, J., Grannec, F., Patey, M. D., Vicars, W., Alexander, B., Achterberg, E. P., (2013). Isotopic composition of atmospheric nitrate in a tropical marine boundary layer. Proceedings of the National Academy of Sciences, 110(44), 17668–17673. https://doi.org/10.1073/pnas.1216639110

Sharma, H. D., Jervis, R. E., & Wong, K. Y. (1970). Isotopic exchange reactions in nitrogen oxides. The Journal of Physical Chemistry, 74(4), 923–933. https://doi.org/10.1021/j100699a044

Takei, T., Yamazaki, A., Watanabe, T., & Chikazawa, M. (1997). Water adsorption properties on porous silica glass surface modified by trimethylsilyl groups. Journal of Colloid and Interface Science, 188(2), 409–414. https://doi.org/10.1006/jcis.1997.4777

Urey, H. C. (1947). The thermodynamic properties of isotopic substances. Journal of the Chemical Society (Resumed), 562-581. https://doi.org/10.1039/JR9470000562

Vicars, W. C., Morin, S., Savarino, J., Wagner, N. L., Erbland, J., Vince, E., Martins, J. M. F., Lerner, B. M., Quinn, P. K., Coffman, D. J., Williams, E. J., Brown, S. S., (2013). Spatial and diurnal variability in reactive nitrogen oxide chemistry as reflected in the isotopic composition of atmospheric nitrate: Results from the CalNex 2010 field study. Journal of Geophysical Research: Atmospheres, 118(18), 10–567. https://doi.org/10.1002/jgrd.50680

Walters, W. W., & Michalski, G. (2015). Theoretical calculation of nitrogen isotope equilibrium exchange fractionation factors for various $NO_y$ molecules. Geochimica et Cosmochimica Acta, 164, 284–297. https://doi.org/10.1016/j.gca.2015.05.029

Walters, W. W., Goodwin, S. R., & Michalski, G. (2015). Nitrogen stable isotope composition ($\delta^{15}N$) of vehicle-emitted $NO_x$. Environmental Science & Technology, 49(4), 2278–2285. https://doi.org/10.1021/es505580v

Walters, W. W., & Michalski, G. (2016). Ab initio study of nitrogen and position-specific oxygen kinetic isotope effects in the $NO+O_3$ reaction. The Journal of chemical physics, 145(22), 224311. https://doi.org/10.1063/1.4968562

Walters, W. W., Simonini, D. S., & Michalski, G. (2016). Nitrogen isotope exchange between NO and $NO_2$ and its implications for $\delta^{15}N$ variations in tropospheric $NO_x$ and atmospheric nitrate. Geophysical Research Letters, 43(1), 440–448. https://doi.org/10.1002/2015GL066438

Walters, W. W., Fang, H., & Michalski, G. (2018). Summertime diurnal variations in the isotopic composition of atmospheric nitrogen dioxide at a small midwestern United States city. Atmospheric Environment, 179, 1–11. https://doi.org/10.1016/j.atmosenv.2018.01.047

Williams, E. L., & Grosjean, D. (1990). Removal of atmospheric oxidants with annular denuders. Environmental Science & Technology, 24(6), 811–814. https://doi.org/10.1021/es00076a002

Yang, J., Honrath, R. E., Peterson, M. C., Dibb, J. E., Sumner, A. L., Shepson, P. B., Frey, M., Jacobi, H.-W., Swanson, A., Blake, N., (2002). Impacts of snowpack emissions on deduced levels

of OH and peroxy radicals at Summit, Greenland. Atmospheric Environment, 36(15–16), 2523–2534. https://doi.org/10.1016/S1352-2310(02)00128-0

Zhang, X., Ortega, J., Huang, Y., Shertz, S., Tyndall, G. S., & Orlando, J. J. (2018). A steady-state continuous flow chamber for the study of daytime and nighttime chemistry under atmospherically relevant NO levels. Atmospheric Measurement Techniques, 11(5), 2537–2551. https://doi.org/10.5194/amt-11-2537-2018

Zong, Z., Wang, X., Tian, C., Chen, Y., Fang, Y., Zhang, F., Li, C., Sun, J., Li, J., Zhang, G., (2017). First assessment of $NO_x$ sources at a regional background site in North China using isotopic analysis linked with modeling. Environmental Science & Technology, 51(11), 5923–5931. https://doi.org/10.1021/acs.est.6b06316

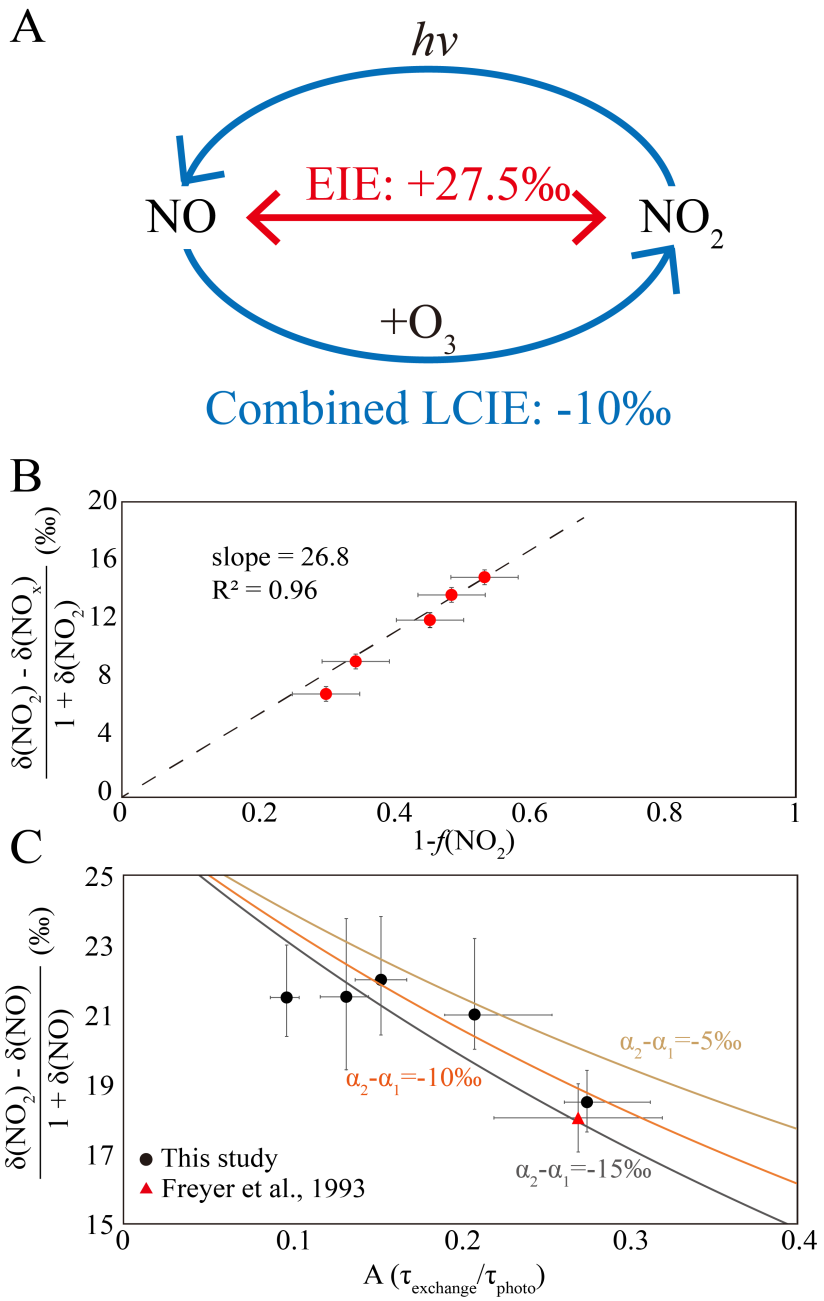


**Fig. 1 A.** a sketch of the isotopic fractionation processes between NO and $NO_2$, both fractionation factors are determined in this work. **B.** Results from five dark experiments yielded a line with slope of 0.0268 and an $\alpha(NO_2\text{-}NO)$ value of 1.0275; **C.** Results from five UV irradiation experiments (black points) and a previous field study (red triangle). The three lines represent different $(\alpha_2\text{-}\alpha_1)$ values: the $(\alpha_2\text{-}\alpha_1)$=-10 ‰ line showed the lowest RMSE to our experimental data as well as the previous field observation. The error bars in panels B and C represented the combined uncertainties of $NO_x$ concentration measurements and isotopic analysis.

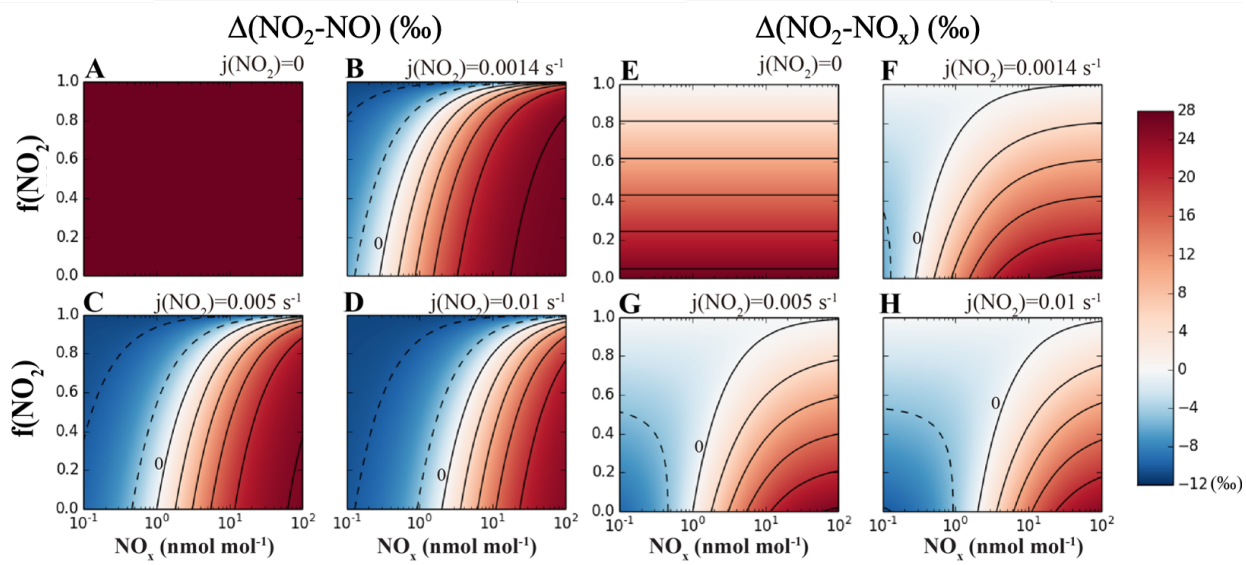


**Fig. 2** Calculating isotopic fractionation values between NO-$NO_2$ ($\Delta(NO_2\text{-}NO)$, **A-D**) and $NO_x$-$NO_2$ ($\Delta(NO_2\text{-}NO_x)$, **E-H**) at various $j(NO_2)$, $NO_x$ level and $f(NO_2)$ using Eq. (7) and (8). Each panel represents a fixed $j(NO_2)$ value (showing on the upper right side of each panel), and the fractionation values are shown by color. Lines are contours with the same fractionation values, at an interval of 5‰, the contour line representing 0‰ was marked on each panel except for A and E.

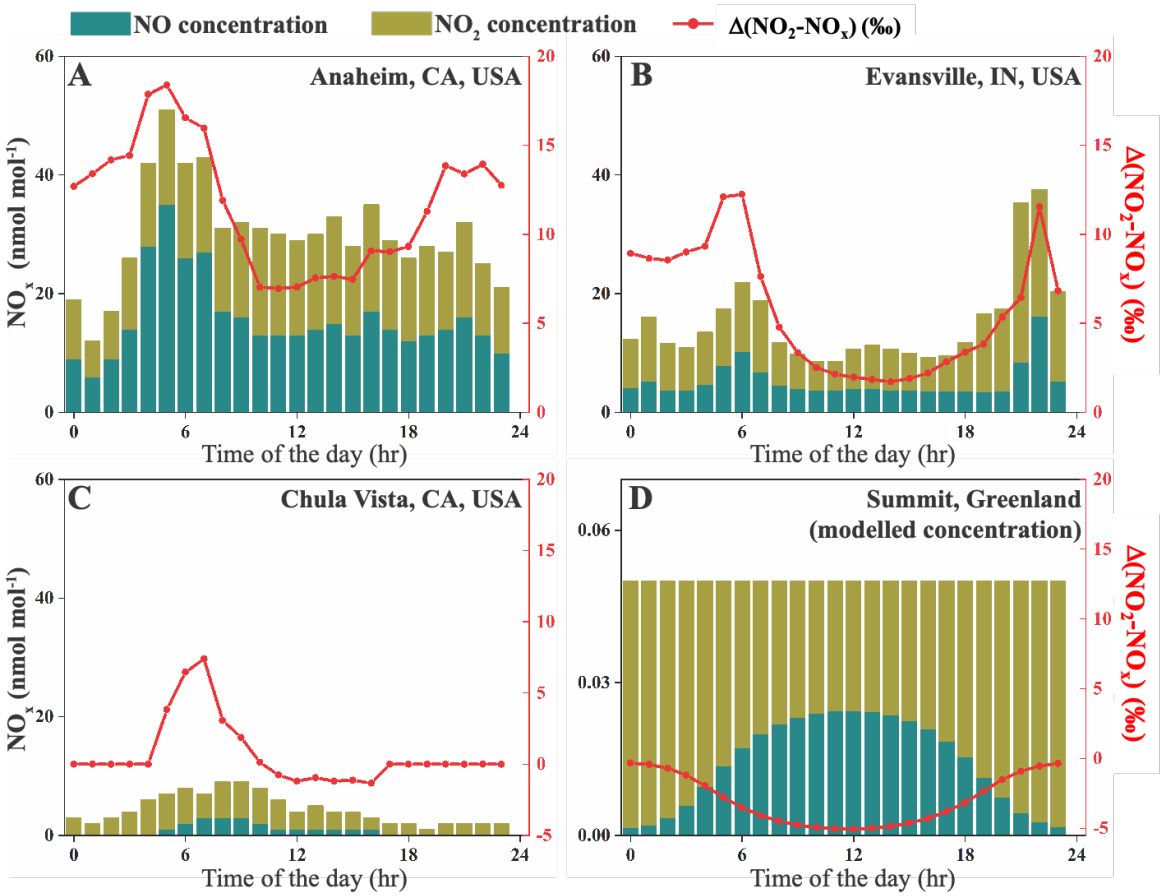


**Fig. 3** $NO_x$ concentrations and calculated $\Delta(NO_2\text{-}NO_x)$ values at four sites. Stacked bars show the NO and $NO_2$ concentrations extracted from monitoring sites (A-C) or calculated using 0-D box model (D); the red lines are $\Delta(NO_2\text{-}NO_x)$ values at each site. Note that the $NO_x$ concentration (left-y) axis on panel D is different from the rest.

## Appendix A. Chamber descriptions

The chamber is a 10 $m^3$ Teflon bag equipped with several standard instruments including temperature and humidity probe, $NO_x$ monitor and $O_3$ monitor. 128 wall-mounted blacklight tubes surrounded the chamber to mimic tropospheric photochemistry and the photolysis rate of $NO_2$ ($j(NO_2)$) when all lights are on have been previously determined to be $1.4\times10^{-3}$ $s^{-1}$, similar to a $j(NO_2)$ coefficient at an 81-degree solar zenith angle. The irradiation spectrum of the blacklights are shown in Figure A1. The chamber was kept at room temperature and one atmospheric pressure. Before each experiment, the chamber was flushed with zero air at 40 L $min^{-1}$ for at least 12 hours to ensure the background $NO_x$, $O_3$ and other trace gases were below detection limit.

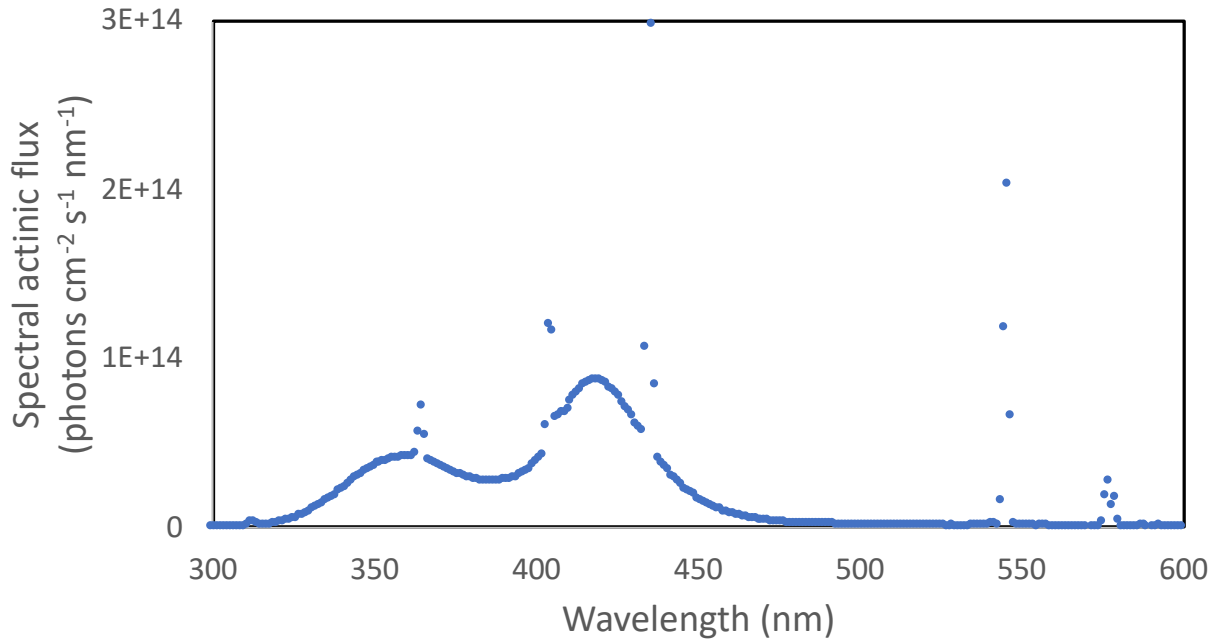


Figure A1 Spectral actinic flux versus wavelengths of the UV light source used in our experiments.

## Appendix B. Box model assessing the time needed for $NO$-$NO_2$ to reach isotopic equilibrium

The time needed to reach $NO$-$NO_2$ isotopic equilibrium during light-off experiments were assessed using a 0-D box model. This box model contains only two reactions:

$^{15}NO_2 + {}^{14}NO \rightarrow {}^{15}NO + {}^{14}NO_2$ $\quad k = 8.14000 \times 10^{-14}\ cm^3\ s^{-1}$

$^{15}NO + {}^{14}NO_2 \rightarrow {}^{15}NO_2 + {}^{14}NO$ $\quad k' = 8.36385 \times 10^{-14}\ cm^3\ s^{-1}$

Where k and k' are rate constants of the reactions. The differences in rate constants were calculated by assuming an $\alpha(NO_2\text{-}NO)$ value of 1.0275. Six simulations were conducted at various initial NO (with $\delta^{15}N = 0‰$) and $O_3$ levels that were similar to our experiment. Then the $\delta^{15}N$ values of NO and $NO_2$ during the simulation were calculated from the model and were shown in Figure B1, suggesting that in our experimental condition, all systems should reach isotopic equilibrium within 1 hr.

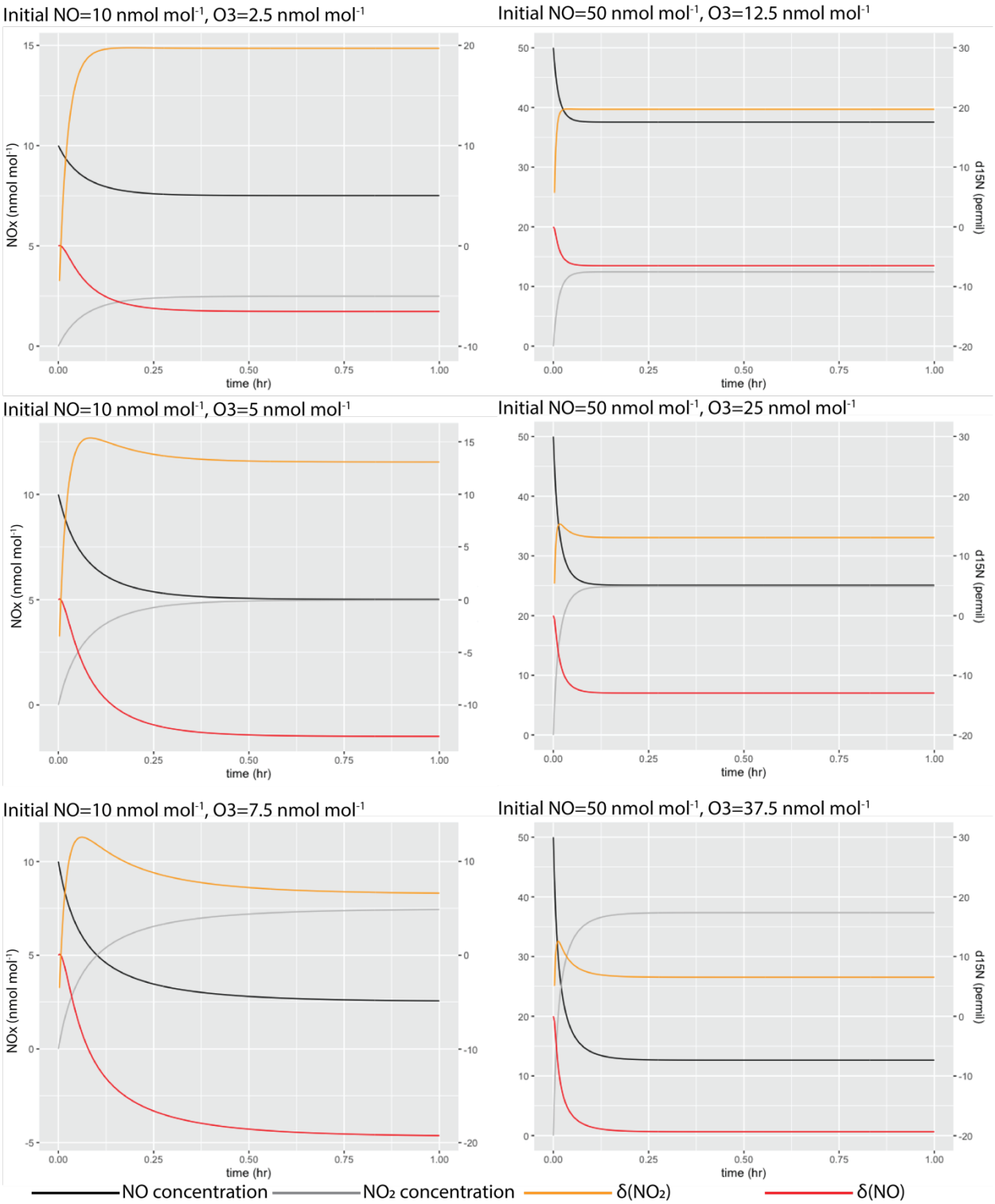


Figure B1 Simulated NO-$NO_2$ isotopic equilibrium process in the chamber at various NO and $O_3$ concentrations.

## Appendix C. Deriving Equations 7 and 8

When the system (R1-R6) reaches steady-state, we have:

$$d[^{15}NO_2]/dt=0 \quad \text{Eq. (C1)}$$

Therefore, using R1-R6:

$$k_1 [^{15}NO_2][^{14}NO]+j(NO_2)\alpha_1[^{15}NO_2]=$$

$$k_5\alpha_2[^{15}NO][O_3]+ k_1\alpha(NO_2\text{-}NO) [^{15}NO][^{14}NO_2] \quad \text{Eq. (C2)}$$

From here we refer $^{14}NO_2$ and $^{14}NO$ as $NO_2$ and NO for convenience, rearrange the above equation, we get:

$$\frac{[^{15}NO_2]}{[^{15}NO]} = \frac{k_5\alpha_2[O_3]+k_1\alpha(NO_2-NO)\,[NO_2]}{j_{NO2}\alpha_1+k_1[NO]} \quad \text{Eq. (C3)}$$

Meantime, since the Leighton cycle reaction still holds for the majority isotopes (NO and $NO_2$), we have:

$$j_{NO2}[NO_2]= k_5[NO][O_3] \quad \text{Eq. (C4)}$$

Thus,

$$\frac{[NO_2]}{[NO]} = \frac{k_5\times[O_3]}{j_{NO2}} \quad \text{Eq. (C5)}$$

From the text, when $j_{NO2}>0$, we defined $A=\tau_{exchange}/\tau_{photo}=j_{NO2}/(k_1\times[NO])$. Using the above equations, we know:

$$\frac{j_{NO2}}{[NO]} = \frac{k_5[O_3]}{[NO_2]} = Ak_1 \quad \text{Eq. (C6)}$$

$$\frac{j_{NO2}}{k_1[NO]} = \frac{k_5[O_3]}{k_1[NO_2]} = A \quad \text{Eq. (C7)}$$

Next, to calculate $\delta(NO_2)$-$\delta(NO)$, we use the definition of delta notation:

$$\delta(NO_2)\text{-}\delta(NO) = R_{NO2}/R_{std}\text{-}\ R_{NO}/R_{std} = (R_{NO2}/R_{NO}\text{-}1)(1+\delta(NO)) \quad \text{Eq. (C8)}$$

$$\frac{R_{NO2}}{R_{NO}} = \frac{[^{15}NO_2][NO]}{[^{15}NO][NO_2]} = \frac{k_5\alpha_2[O_3][NO]+k_1\alpha(NO_2-NO)[NO_2][NO]}{j_{NO2}\alpha_1[NO_2]+k_1[NO][NO_2]} \quad \text{Eq. (C9)}$$

Divide both side by $k_1[NO][NO_2]$:

$$\frac{R_{NO2}}{R_{NO}} = \frac{\frac{k_5\alpha_2[O_3]}{k_1[NO_2]}+\alpha(NO_2-NO)}{\frac{j_{NO2}\alpha_1}{k_1[NO]}+1} \quad \text{Eq. (C10)}$$

Rearrange and substitute $\frac{k_5[O_3]}{k_1[NO_2]}$ and $\frac{j_{NO2}}{k_1[NO]}$ with A:

$$\frac{R_{NO2}}{R_{NO}} = \frac{\alpha_2\times A+\alpha(NO_2-NO)}{\alpha_1\times A+1} \quad \text{Eq. (C11)}$$

$$\frac{R_{NO2}}{R_{NO}} - 1 = \frac{(\alpha_2-\alpha_1)\times A+(\alpha(NO_2-NO)-1)}{\alpha_1\times A+1} \quad \text{Eq. (C12)}$$

Thus,

$$\delta(NO_2)\text{-}\delta(NO)=\frac{(\alpha_2-\alpha_1)\times A+(\alpha(NO_2-NO)-1)}{\alpha_1\times A+1}(1+\delta(NO)) \quad \text{Eq. (C13)}$$

Since $\alpha_1 \approx 1$, $\alpha_1\times A+1 \approx 1+A$ this equation can be further simplified to Eq. 7:

$$\delta(NO_2)\text{-}\delta(NO)=\frac{(\alpha_2-\alpha_1)*A+\alpha(NO_2-NO)-1)}{A+1}(1+\delta(NO)) \quad \text{Eq. (C14)}$$

Then, using mass balance:

$$\delta(NO_2)\, f(NO_2)+\delta(NO)(1- f(NO_2)) = \delta(NO_x) \quad \text{Eq. (C15)}$$

We can derive Eq. 8:

$$\delta(NO_2)\text{-}\delta(NO_x)=\frac{(\alpha_2-\alpha_1)\times A+\alpha(NO_2-NO)-1)}{A+1}\,(1+\delta(NO))\,(1- f(NO_2)) \quad \text{Eq. (C16)}$$